Supplemental Information for "Fresnel reflection from a cavity with net roundtrip gain"

Tobias S. Mansuripur[1,*] and Masud Mansuripur[2]

[1] *Department of Physics, Harvard University, Cambridge, MA 02139*

[2] *College of Optical Sciences, The University of Arizona, Tucson, AZ 85721*

[*] mansuripur@physics.harvard.edu

I. PRESCRIPTION FOR R AND L SUPERSCRIPTS

The energy flux of an s-polarized planewave whose E-field is given by

$$E_y(x,z,t) = E_0 \exp(ik_x x + ik_z z - i\omega t) \tag{1}$$

in a medium (ϵ, μ) is given by the time-average of the Poynting vector $\boldsymbol{S} \equiv \vec{E} \times \vec{H}$,

$$\langle \vec{S} \rangle = \frac{|E_0|^2}{2\omega\mu_0} e^{-2\mathrm{Im}(k_z)z} \left(\mathrm{Re}\left[\frac{k_x}{\mu}\right] \hat{x} + \mathrm{Re}\left[\frac{k_z}{\mu}\right] \hat{z} \right). \tag{2}$$

Therefore, energy flows in the $+z$-direction ('to the right,' in our convention) when $\mathrm{Re}(k_z/\mu) > 0$, and we denote the wavevector k_z which satisfies this condition with the superscript R. Any value k_z for which $\mathrm{Re}(k_z/\mu) < 0$ is accordingly labeled with a superscript L. It follows from these definitions that k_z^R must make an acute angle with μ in the complex plane. (For p-polarized light energy flows in the $+z$-direction when $\mathrm{Re}(k_z/\epsilon) > 0$, and so k_z^R makes an acute angle with ϵ in the complex plane.)

In cases where $\langle S_z \rangle = 0$, we must establish a prescription for resolving the ambiguity in the choice of superscript, which is best illustrated by an example. Consider the case where medium one is a lossless dielectric ($\epsilon_1 > 1$, $\mu_1 = 1$), medium two is vacuum, and the incident propagating wave satisfies $k_x > k_0$, where $k_0 \equiv \omega/c$, so that the two choices for k_{2z} are $\pm i\sqrt{k_x^2 - k_0^2}$. Both choices for k_{2z} yield pure evanescent waves and carry no energy along the z-direction. By adding a small amount of loss to medium two, so that $\epsilon_2 = 1 + i\epsilon_2''$ where $\epsilon_2'' > 0$, the two choices for k_{2z} deviate slightly from the imaginary axis as shown in Fig. S1(a). Now both waves carry non-zero energy along the z-direction; the first quadrant solution is k_{2z}^R (which can be seen quickly because it makes an acute angle with $\mu_2 = 1$) and the third quadrant solution is k_{2z}^L. Our prescription to establish k_{2z}^R for a true vacuum (i.e., $\epsilon_2'' = 0$) is to take the limit $\epsilon_2'' \to 0$, which yields k_{2z}^R as the solution along the positive imaginary axis.

Beware that if one adds a small amount of gain rather than loss to medium two, so that $\epsilon_2 = 1 + i\epsilon_2''$ where $\epsilon_2'' < 0$, then the two solutions for k_{2z} exist in the second and fourth quadrants as shown in Fig. S1(b), and in this case k_{2z}^R points predominantly along the *negative* imaginary axis. Thus, we see that the two limiting cases as gain or loss approaches zero do not yield the same result:

$$\lim_{\epsilon_2'' \to 0^+} k_{2z}^R = -\lim_{\epsilon_2'' \to 0^-} k_{2z}^R. \tag{3}$$

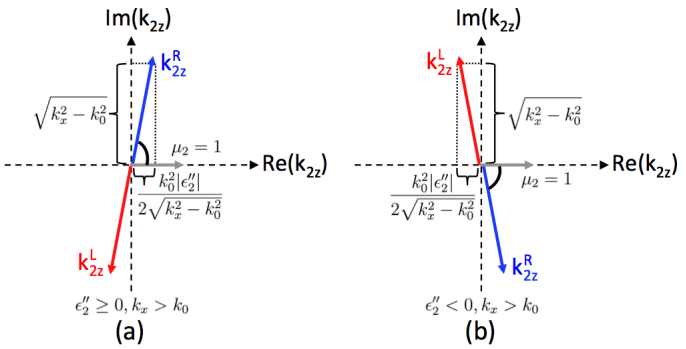

FIG. S1. Choosing the R or L label for an evanescent wave. (a) The two choices for k_{2z} are shown for the case of a slightly "lossy vacuum" ($\epsilon_2 = 1 + i\epsilon_2''$ where $\epsilon_2'' > 0$, $\mu_2 = 1$), for the case $k_x > k_0$. The first quadrant solution carries energy to the right and is labeled k_{2z}^R, and our prescription is to take the limit $\epsilon_2'' \to 0$ to determine that k_{2z}^R in the lossless case is along the positive imaginary axis. (b) For a slightly "gainy vacuum" ($\epsilon_2'' < 0$) the two solutions for k_{2z} are in the second and fourth quadrants, and k_{2z}^R approaches the negative imaginary axis as $\epsilon_2'' \to 0$. The magnitudes of the real and imaginary parts of k_{2z} in (a) and (b) are approximated using the first order Taylor expansion for small ϵ_2'': $k_0^2|\epsilon_2''| \ll k_x^2 - k_0^2$.

To have an unambiguous labeling convention for the case $\epsilon_2'' = 0$, we emphasize that one must take the limit as *loss* approaches zero, which can be different from the limit as gain approaches zero in the case of evanescent waves.

Finally, it is worth noting that this discontinuity in the two limiting cases, apart from being a footnote in establishing a labeling convention, is actually at the heart of the debate over single-surface amplified TIR. When medium two has gain, if one chooses k_{2z}^R as the transmitted wavevector (in accordance with our postulate), then it seems unphysical that as the gain approaches (but does not reach) zero the transmitted wave should still be strongly amplified. To remedy this situation it has been suggested that the correct choice for the transmitted wavevector should be k_{2z}^L when medium two has gain and $k_x > k_0$, so that the transmitted wave decays in the $+z$-direction. We believe, instead, that the discontinuity in the two limits is not as unphysical as it might appear at first: the transmitted wave propagates a large distance in the x-direction while barely moving forward in the z-direction (since $k_x \gg \mathrm{Re}(k_{2z}^R)$), so the large gain in the z-direction is actually a result of the long propagation distance along the x-direction. Far more unphysical, in our opinion, is the decision to switch the transmitted wavevector from k_{2z}^R when $k_x < k_0$ to k_{2z}^L when $k_x > k_0$.

All of these arguments aside, however, the purpose of our paper has been to demonstrate the Fresnel mechanism by which the specularly reflected beam from a finite-thickness slab is amplified, both below and above the critical angle.

II. GAIN SATURATION

Physicists familiar with the principles of lasers should be rightfully wary of a steady-state solution with roundtrip coefficient $|\nu|$ greater than one. When an active medium is pumped strongly enough to generate a sufficiently large population inversion to yield $|\nu|$ greater than one, light initially generated by spontaneous emission in the cavity will be amplified after each roundtrip. However, the field amplitude does not grow without bound–as the field gains strength the upper state lifetime is reduced by stimulated emission, which causes the population inversion to decrease to a level such that $\nu = 1$, resulting in steady-state lasing. This gain reduction with increasing field amplitude is known as gain saturation. In a laser, therefore, the situation $|\nu| > 1$ is only a transient state. It clearly cannot be a steady-state solution, because the field would grow without bound.

The situation changes when we allow an incident wave to strike the active medium, as we do in this paper. Note that ν is defined as the roundtrip coefficient *in the absence of an incident wave*; that is, the reflectivity r_{21} is calculated by assuming that there is no wave in medium one arriving at the cavity. To account for the incident wave, we can define an effective facet reflectivity at the two-one interface $r_{21}^{\text{eff}} \equiv E_2^R/E_2^L$. Furthermore, we can define an effective roundtrip coefficient in the slab which replaces r_{21} with r_{21}^{eff}, that is, $\nu^{\text{eff}} = r_{21}^{\text{eff}} r_{23} \exp(2ik_{2z}^R d)$. We emphasize that *every possible steady-state solution to the problem under consideration, whether the slab is passive or active, and whether there is an incident wave or not, satisfies the condition* $\nu^{\text{eff}} = 1$. This is a fundamental property of steady-state solutions: the field in the slab must regenerate itself after every roundtrip, once all sources and sinks have been accounted for. Therefore, in situations where $|\nu| > 1$, the incident wave must, upon transmission into medium two, interfere destructively with the circulating field in the slab so that $|r_{21}^{\text{eff}}| < |r_{21}|$, which ultimately forces ν^{eff} toward 1. In summary, when there is no incident wave the situation $|\nu| > 1$ is temporary because the field will grow until gain saturation (a nonlinear effect) forces the $\nu = 1$ solution. With an incident wave, a linear steady-state solution is possible even when $|\nu| > 1$ because of the

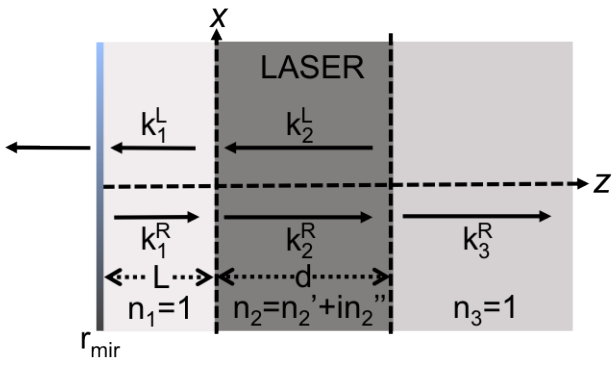

FIG. S2. Schematic of a laser with self-feedback. A mirror of reflectivity r_{mir} allows light emitted by medium two to be re-injected. The feedback alters the laser threshold, and can be modeled by an effective facet reflectivity r_{21}^{eff}, which differs from the bare facet reflectivity r_{21} in the absence of feedback.

reduction in the effective facet reflectivity r_{21}^{eff}, which prevents the unbounded growth of the fields so that one does not have to rely on gain saturation to avoid a nonphysical divergence.

An example that illustrates well the distinction between ν and ν^{eff} is a laser subject to self-feedback, shown in Fig. S2. In this case, the laser (medium 2) emits light in a direction normal to both of its facets, and a mirror of reflectivity r_{mir} placed a distance L from the left facet reflects some of the laser output and creates the wavevector $\mathbf{k}_1^R$, which is then reinjected into the laser. (To be clear, this is different from the situation considered in our paper, for which $\mathbf{k}_1^R$ is generated by an external source.) For a suitable choice of L and r_{mir}, the re-injected wave will interfere destructively with the circulating field in the gain medium, effectively reducing the reflection coefficient at the 2-1 interface without altering its phase. Specifically, for $n_1 = 1$ and $n_2 = n_2' + in_2''$, the facet reflectivity in the absence of feedback is $r_{21} = (n_2 - 1)/(n_2 + 1)$. The feedback from the external mirror will reduce the effective reflection coefficient to $r_{21}^{\text{eff}} = \alpha r_{21}$, where α is real and satisfies $0 \leq \alpha \leq 1$, provided r_m and L are chosen such that

$$r_m \exp(i4\pi L/\lambda_o) = \frac{(1-\alpha)r_{21}}{\alpha r_{21}^2 - 1}. \tag{4}$$

So long as $|r_{21}| < 1$ (which is generally the case), it is possible to choose r_m and L so that $|r_m| < 1$, i.e., the external mirror is a simple, passive component. As an application of Eq. 4, consider the case $n_2 = 1.5 - 0.01i$ and $\lambda_o = 1$ μm. The bare facet reflectivity is $r_{21} = 0.2\exp(-0.016i)$. If we want the effective facet reflectivity to be $r_{21}^{\text{eff}} = 0.1\exp(-0.016i)$

(half the magnitude but the same phase as the bare facet reflectivity), we choose $\alpha = 0.5$ and find that we should place a mirror of reflectivity $r_m = -0.102$ a distance $L = 0.499$ μm from the left facet.

Because the external mirror reduces the effective facet reflectivity so that $|r_{21}^{\text{eff}}| < |r_{21}|$, the effective roundtrip coefficient $|\nu^{\text{eff}}|$ will be less than $|\nu|$. When medium two is pumped beyond the lasing threshold, ν^{eff} will be clamped to 1, which means that $|\nu|$ will be greater than 1. There also exists a subthreshold pumping regime for which $|\nu| > 1$. The example of the laser with self-feedback demonstrates that an active cavity subject to an incident field can have a roundtrip coefficient ν with magnitude greater than 1, and that this situation is neither transient nor unstable.

In the above example, there is always a well-defined phase relationship between the field circulating in the laser and the re-injected field. This will not necessarily be true when the incident wave is generated by an external source: spontaneous emission, being a stochastic process, can give rise to a field within medium two that has no well-defined phase relationship with the incident wave. Whether this leads to instabilities remains to be decisively answered, but we note that the existing experimental evidence in the $|\nu| > 1$ regime has not, to our knowledge, detected any instabilities [14, 20, 21]. It is also worth commenting on an important difference between spontaneously-emitted cavity-photons traveling parallel to the surface-normal of the cavity facets versus those emitted at an oblique angle to the optical axis. For photons emitted parallel to the surface-normal, the slab is clearly a cavity that provides feedback, as the light retraces its path on every roundtrip. However, as mentioned in the main text, the roundtrip coefficient is a function of incidence angle, and for the material parameters used for Fig. 2(b), $|\nu|$ exceeds one only for incidence angles $\theta > 27.43°$. In particular, this means that $|\nu| < 1$ for $\theta = 0$; therefore, the gain is insufficient for a spontaneously emitted cavity photon in the $\theta = 0$ direction to cause lasing. In contrast, a cavity photon emitted spontaneously at a large θ such that $|\nu| > 1$ would seem to experience net amplification after each roundtrip. (We say 'seem to' because this is the intuitive interpretation to us; however, we mention again that the experiments that have probed the regime of $|\nu| > 1$ have not detected such problems with spontaneous emission [14, 20, 21].) Should these obliquely-traveling spontaneously-emitted photons prove problematic in a future experiment, however, they will anyway exit the slab at the top and bottom facets, since any real slab must have a finite length in the x-direction. One could also coat the top and

bottom facets with broadband antireflection coatings to facilitate this removal; this way, these spontaneously emitted photons would leave the slab before they are amplified to the point where they saturate the gain. We mention this only as a consideration for a potential experiment that looks for the pre-excitation mechanism. Our intent in this Letter has been to explore the predictions of the Fresnel solution for a slab with $|\nu| > 1$; in the end, only experiments can decide whether this solution is physical.

III. PULSE OF LIGHT INCIDENT ON GAINY SLAB WITH $|\nu| > 1$

The video file pulse_video.mov included online is a time-lapse video of $|E_y|^2$ of a pulse of light, rather than a beam, for the same material parameters as in Fig. 2(b) of the main text: $\epsilon_1 = \epsilon_3 = 2.25$, $\epsilon_2 = 1 - 0.01i$, $\mu_1 = \mu_2 = \mu_3 = 1$, $d = 28$ μm. The white vertical lines in the video identify the 1-2 and 2-3 interfaces. The incident pulse is s-polarized and Gaussian in both space (FWHM = 13.3 μm) and time (FWHM = 50 fs, or 15 optical cycles). The central wavelength of the pulse is $\lambda_o = 1$ μm, and the mean incidence angle (i.e., averaged over all constituent planewaves) is 30°. The size of each video frame is 210 μm by 150 μm (height by width). The time elapsed between frames is 10 fs, and the entire video spans 1.22 ps (123 frames total). The field $|E_y|^2$ is plotted on a logarithmic scale covering 3 decades, i.e. red corresponds to the maximum intensity and blue corresponds to intensities less than or equal to 1/1000th of the maximum. The background in this image is blue, which corresponds to the minimum of $|E_y|^2$, whereas the background in Figs. 2(a) and 2(b) is green because it is the field E_y that was plotted in that case, so that blue corresponded to the maximum negative field.

In the video, one first sees the incident pulse near the bottom left of the screen, traveling up and to the right. The pre-excitation is soon seen in the slab at the bottom of the frame, and the reflected pulse that corresponds to the $m = 1$ term in the primed partial wave expansion leaves the slab and propagates up and to the left in medium one. The pre-excitation in the slab then undergoes one roundtrip as it zig-zags upward, giving rise to a transmitted pulse in medium three followed by the $m = 0$ reflected pulse in medium one. The pre-excitation then makes one more roundtrip, giving rise to another transmitted pulse in medium three, and then approaches the two-one interface at the same time the incident pulse arrives from the opposite side. The two pulses interfere in such a way as to yield an

amplified specularly reflected pulse by entirely depleting the energy content of the slab. The fact that the pre-excitation in the slab travels in the $+x$-direction clearly distinguishes this behavior from negative refraction.

IV. DESCRIPTION OF SIMULATION

The E-field plots of the Gaussian beams and the video of the pulse were created using MATLAB. The field at each pixel is determined by superposing a large (but of course finite) number of planewave solutions. Therefore, the plots represent analytical solutions to Maxwell's equations.

As described in the main text, the response of the slab to an incident s-polarized planewave with amplitude E_1^R and wavevector $\boldsymbol{k}_1^R = k_x\hat{\boldsymbol{x}} + k_{1z}^R\hat{\boldsymbol{z}}$ is given by

$$E_y(x,z) = \begin{cases} E_1^R \exp(ik_x x + ik_{1z}^R z) + E_1^L \exp(ik_x x + ik_{1z}^L z) & : z \le 0 \\ E_2^R \exp(ik_x x + ik_{2z}^R z) + E_2^L \exp(ik_x x + ik_{2z}^L z) & : 0 \le z \le d \\ E_3^R \exp[ik_x x + ik_{3z}^R (z-d)] & : z \ge d \end{cases} \tag{5}$$

and the time-dependence factor $\exp(-i\omega t)$ is not explicitly written. The wavevector components k_{2z}^R and k_{3z}^R are determined by the dispersion relation

$$k_{\ell z}^R = \sqrt{(\omega/c)^2 \mu_\ell \epsilon_\ell - k_x^2}, \tag{6}$$

where μ_ℓ and ϵ_ℓ are the relative magnetic permeability and electric permittivity constants of material ℓ, and the sign of the square root is chosen according to the prescription described in Supplementary Sec. 1. The four unknown wave amplitudes are found by satisfying Maxwell's boundary conditions to be

$$E_2^R = \frac{2k_{1z}^R(k_{3z}^R + k_{2z}^R)E_1^R}{(k_{2z}^R + k_{1z}^R)(k_{3z}^R + k_{2z}^R) + \exp(2ik_{2z}^R d)(k_{3z}^R - k_{2z}^R)(k_{2z}^R - k_{1z}^R)} \tag{7}$$

$$E_2^L = \frac{-2k_{1z}^R(k_{3z}^R - k_{2z}^R)E_1^R}{(k_{2z}^R - k_{1z}^R)(k_{3z}^R - k_{2z}^R) + \exp(-2ik_{2z}^R d)(k_{3z}^R + k_{2z}^R)(k_{2z}^R + k_{1z}^R)} \tag{8}$$

$$E_1^L = E_2^R + E_2^L - E_1^R \tag{9}$$

$$E_3^R = E_2^R \exp(ik_{2z}^R d) + E_2^L \exp(-ik_{2z}^R d). \tag{10}$$

To construct the Gaussian beam from the planewave solutions, we begin by expressing E_y in the $z = 0$ plane for a beam traveling parallel to the z-axis

$$E_y(x, z=0) = E_0 \exp\left(-\frac{x^2}{2\sigma_x^2}\right), \tag{11}$$

where E_0 is the peak amplitude and σ_x is directly proportional to the spatial FWHM

$$w_x = 2\sqrt{2\ln 2}\sigma_x. \tag{12}$$

By Fourier transforming and subsequently inverting the transform, the field can equivalently be written as an integral in k-space,

$$E_y(x, z = 0) = \int_{-\infty}^{\infty} dk_x E_1^R(k_x) \exp(ik_x x), \tag{13}$$

where

$$E_1^R(k_x) = \frac{E_0\sigma_x}{\sqrt{2\pi}} \exp\left(\frac{-k_x^2}{2(1/\sigma_x)^2}\right), \tag{14}$$

and the FWHM in k-space is

$$w_k = 2\sqrt{2\ln 2}/\sigma_x. \tag{15}$$

To propagate the beam beyond the $z = 0$ plane, we associate with each value of k_x a component k_{1z}^R such that the total wavevector obeys the dispersion relation in medium one,

$$k_{1z}^R(k_x) = \sqrt{(\omega/c)^2\mu_1\epsilon_1 - k_x^2}. \tag{16}$$

Now the Gaussian beam can be expressed as a function of x and z by

$$E_y(x, z) = \int_{-\infty}^{\infty} dk_x E_1^R(k_x) \exp[i(k_x x + k_{1z}^R z)]. \tag{17}$$

At this point, we must approximate the integral in Eq. 17 by discretization so that the calculation can be carried out by a computer. We restrict k_x to a finite sampling width w_s given by $-w_s/2 \leq k_x \leq w_s/2$, and sample the beam equidistantly within this region with a total number of samples N_s. The integral in Eq. 17 is approximated by the sum

$$E_y(x, z) = \sum_{k_x=-w_s/2}^{w_s/2} \Delta k_x E_1^R(k_x) \exp[i(k_x x + k_{1z}^R z)], \tag{18}$$

where

$$\Delta k_x = \frac{w_s}{N_s - 1}. \tag{19}$$

At this point, it is helpful to think of E_1^R, k_x, and k_{1z}^R as vectors containing N_s numerical elements each. To rotate the beam so that it travels at an angle θ to the z-axis, we perform the transformation

$$k_x \to \cos(\theta)k_x + \sin(\theta)k_z \tag{20}$$

$$k_{1z}^R \to -\sin(\theta)k_x + \cos(\theta)k_{1z}^R \tag{21}$$

on each element of k_x and k_{1z}^R. (The Fourier amplitude of each plane-wave $E_1^R(k_x)$ is unaffected by the rotation in the case of s-polarized light.) Finally, to displace the waist of the beam to some location (x_0, z_0) in the incidence medium, one must multiply each Fourier amplitude by

$$E_1^R(k_x) \rightarrow E_1^R(k_x) \exp[-i(k_x x_0 + k_{1z}^R z_0)]. \tag{22}$$

With these redefined values for E_1^R, k_x, and k_{1z}^R, the sum in Eq. 18 is a good approximation to a Gaussian beam traveling at an angle θ whose waist is located at (x_0, y_0). The total E-field at any point in the system is given by

$$E_{\text{tot}}(x,z) = \begin{cases} \text{Real}\{\sum \Delta k_x \left(E_1^R(k_x) \exp[i(k_x x + k_{1z}^R z)] + E_1^L(k_x) \exp[i(k_x x + k_{1z}^L z)]\right)\}, & z \leq 0 \\ \text{Real}\{\sum \Delta k_x \left(E_2^R(k_x) \exp[i(k_x x + k_{2z}^R z)] + E_2^L(k_x) \exp[i(k_x x + k_{2z}^L z)]\right)\}, & 0 \leq z \leq d \\ \text{Real}\{\sum \Delta k_x E_3^R(k_x) \exp[i(k_x x + k_{3z}^R z)]\}, & z \geq d \end{cases} \tag{23}$$

where E_1^L, E_2^R, E_2^L, and E_3^R are calculated element-wise from $E_1^R(k_x)$ according to Eqs. 7-10. The beam plots in Fig. 2 of the main text are calculated pixel-by-pixel from the sum in Eq. 23, with the values of x and z indicating the location of the pixel. The resultant field is normalized to the maximum field value in the image, and displayed in color. The pulse video is calculated similarly, except that the field is Gaussian in space and time, and so the field must be sampled in both the spatial and temporal frequency domains. The calculation time is significantly longer for the pulse compared to the beam, and the simulations are only practical to run on a supercomputer.

The finite nature of the sampling has consequences which must be considered in order to be sure that our results are not affected by numerical artifacts. Firstly, the truncation of the Gaussian beam in k-space to the sampling width w_s leads to a convolution with a sinc function in the spatial domain. Therefore, the side-tail of our beam is not truly Gaussian; rather, the envelope of the side-tail is Gaussian but the side-tail itself exhibits periodic sinc-like fluctuations in intensity (which cannot be seen in Fig. 2 of the main text, but can be seen in logarithmic plots which resolve the small intensities of the side-tail). The sampling width chosen for Fig. 2 was $w_s = 2w_k$ (with $N_s = 501$). We made sure that other choices of the sampling width, $w_s = 3w_k$ and $4w_k$ (with proportionally larger N_s so that Δk_x remained constant), did not affect the behavior of the plots. Therefore, our conclusions are not affected by the precise value of the sampling width w_s. Secondly, the finite number of samples N_s

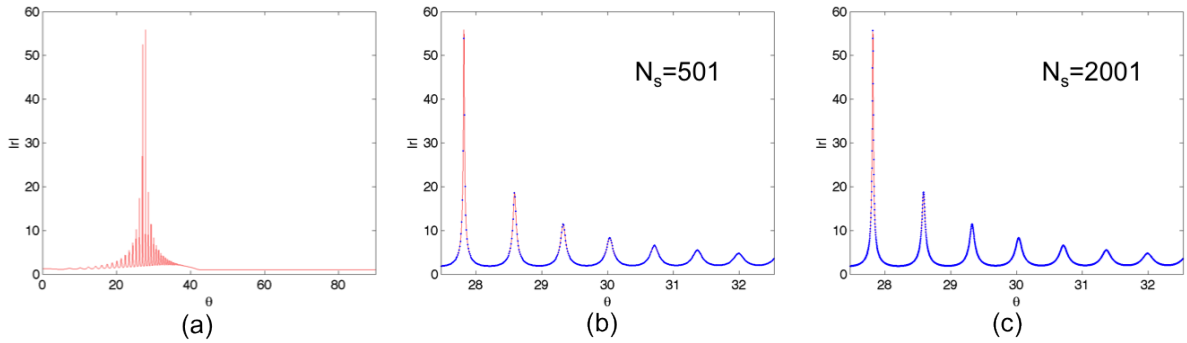

FIG. S3. A pictorial depiction of the Fourier domain sampling used to generate Fig. 2(b) of the main text. (a) A plot of $|r|$ vs. incidence angle θ for the case of $\lambda_o = 1$ μm, ϵ_1=ϵ_3=2.25, $\epsilon_2 = 1 - 0.01i$, and $d = 28$ μm. For a beam-width FWHM of 13.3 μm, the sampling width $w_s = 2w_k$ that we chose restricted the range of incidence angles of the planewaves used to construct the beam to $27.47° < \theta < 32.53°$. In plots (b) and (c), the blue dots overlaying the reflectivity plot indicate the incidence angles of the planewaves that were summed over for (b) $N_s = 501$ samples and (c) $N_s = 2001$ samples. The plot in Fig. 2(b) of the main text looks visually identical for both choices of sampling values.

implies the spectrum of k_x values is discrete, so the incident beam is periodic in space. This means that in the plots of Fig. 2 in the main text, there is not just one incident beam but an infinite number of them impinging on the slab, spaced periodically along the x-axis by a distance $2\pi/\Delta k_x = 2830$ μm. If the sampling is increased from $N_s = 501$ to 2001 while keeping $w_s = 2w_k$ constant (see Fig. S3), the distance between adjacent beams increases to 11330 μm, but the plots in both Figs. 2(a) and 2(b) of the main text look identical to the ones with 501 samples. Therefore, 501 samples is sufficient in this case to ensure that the (periodically repeated) beams do not interfere with each other, and that the plot is a good representation of the field of a single beam.

[1] J.B. Pendry. "Negative refraction makes a perfect lens." Phys. Rev. Lett. **85**, 3966-69 (2000).

[2] D.R. Smith, D. Schuring, M. Rosenbluth, S. Schultz, S.A. Ramakrishna, and J.B. Pendry. "Limitations on subdiffraction imaging with a negative refractive index slab." Appl. Phys. Lett. **82**, 1506-1508 (2003).

[3] N. Garcia and M. Nieto-Vesperinas. "Left-Handed Materials Do Not Make a Perfect Lens." Phys. Rev Lett. **88**, 20, 207403 (2002).

[4] X. Jiang, Q. Li and C.M. Soukoulis. "Symmetry between absorption and amplification in disordered media." Phys. Rev. B **19**, 9007 (1999).

[5] S.A. Ramakrishna. "On the dual symmetry between absorbing and amplifying random media." Pramana **62**, 1273-1279, (2004).

[6] J.C.J. Paasschens, T. Sh. Misirpashaev and C.W.J. Beenakker. "Localization of light: dual symmetry between absorption and amplification." Phys. Rev. B **54**, 11887 (1996).

[7] P. Pradhan and N. Kumar. "Localization of light in coherently amplifying random media." Phys. Rev. B **50**, 9644 (1994).

[8] Z.Q. Zhang. "Light amplification and localization in randomly layered media with gain." Phys. Rev. B **52**, 7960 (1995).

[9] Y. Chen, P. Fischer, and F.W. Wise. "Negative Refraction at Optical Frequencies in Nonmagnetic Two-Component Molecular Media." Phys. Rev. Lett. **95**, (2005).

[10] S.A. Ramakrishna. "Comment on 'Negative Refraction at Optical Frequencies in Nonmagnetic Two-Component Molecular Media.'" Phys. Rev. Lett. **98**, (2007).

[11] S.A. Ramakrishna and O.J.F. Martin. "Resolving the wave vector in negative index media." Opt. Lett. **30**, 19, 2626-2628 (2005).

[12] J.B. Geddes III, T.G. Mackay, and A. Lakhtakia. "On the refractive index for a nonmagnetic two-component medium: Resolution of a controversy." Opt. Comm. **280**, 120-125 (2007).

[13] B. Nistad and J. Skaar. "Causality and elecromagnetic properties of active media." Phys. Rev. E **78**, 036603 (2008).

[14] C.J. Koester. "Laser action by enhanced total internal reflection." IEEE J. Quantum Electron. **QE-2**, 580-4 (1966)

[15] P.R. Callary and C.K. Carniglia. "Internal reflection from an amplifying layer." J. Opt. Sci. Am. **66**, 8 (1976).

[16] J. Fan, A. Dogariu, and L.J. Wang. "Amplified total internal reflection." Opt. Express **11**, 299-308 (2003).

[17] K.J. Willis, J.B. Schneider, and S.C. Hagness. "Amplified total internal reflection: theory, analysis, and demonstration of existence via FDTD." Opt. Express **16**, 1903-14 (2008).

[18] A. Siegman. "Fresnel Reflection and Evanescent Gain." OPN, 38–45 (Jan. 2010).

[19] J.O. Grepstad and J. Skaar. "Total internal reflection and evanescent gain." Opt. Express **19**, 21404 (2011).

[20] E.P. Ippen and C.V. Shank. "Evanescent-field-pumped dye laser." Appl. Phys. Lett. **21**, 301 (1972).

[21] H.H. Choi, H.J. Kim, J. Noh and W. Jhe. "Amplified total internal reflection from a plane dielectric boundary." Jour. Korean Phys. Soc. **42**, 80 (2003).